AFRL-PR-WP-TP-2006-250

INDEPENDENT STAGE CONTROL OF A CASCADE INJECTOR (POSTPRINT)

Heidi L. Meicenheimer, Ephraim J. Gutmark, Campbell D. Carter, Dean R. Eklund, Dr. Mark R. Gruber, and Kuang–Yu Hsu

JULY 2005

Approved for public release; distribution is unlimited.

STINFO COPY

PROPULSION DIRECTORATE
AIR FORCE MATERIEL COMMAND
AIR FORCE RESEARCH LABORATORY
WRIGHT-PATTERSON AIR FORCE BASE, OH 45433-7251

REPORT DOCUMENTATION PAGE

Form Approved
OMB No. 0704-0188

1. REPORT DATE *(DD-MM-YY)*	2. REPORT TYPE	3. DATES COVERED *(From - To)*
July 2005	Conference Paper Postprint	09/01/2004 – 07/31/2005

4. TITLE AND SUBTITLE
INDEPENDENT STAGE CONTROL OF A CASCADE INJECTOR (POSTPRINT)

5a. CONTRACT NUMBER
In-house

5b. GRANT NUMBER

5c. PROGRAM ELEMENT NUMBER
62203F

6. AUTHOR(S)
Heidi L. Meicenheimer and Ephraim J. Gutmark (University of Cincinnati)
Campbell D. Carter, Dean R. Eklund, Dr. Mark R. Gruber (AFRL/PRAS)
Kuang–Yu Hsu (Innovative Scientific Solutions, Inc.)

5d. PROJECT NUMBER
3012

5e. TASK NUMBER
AI

5f. WORK UNIT NUMBER
00

7. PERFORMING ORGANIZATION NAME(S) AND ADDRESS(ES)

University of Cincinnati
Department of Aerospace Engineering
Cincinnati, OH

Propulsion Sciences Branch (AFRL/PRAS)
Aerospace Propulsion Division
Propulsion Directorate
Air Force Research Laboratory
Air Force Materiel Command
Wright-Patterson AFB, OH 45433-7251

Innovative Scientific Solutions, Inc.
Dayton, OH

8. PERFORMING ORGANIZATION REPORT NUMBER
AFRL-PR-WP-TP-2006-250

9. SPONSORING/MONITORING AGENCY NAME(S) AND ADDRESS(ES)
Propulsion Directorate
Air Force Research Laboratory
Air Force Materiel Command
Wright-Patterson AFB, OH 45433-7251

10. SPONSORING/MONITORING AGENCY ACRONYM(S)
AFRL-PR-WP

11. SPONSORING/MONITORING AGENCY REPORT NUMBER(S)
AFRL-PR-WP-TP-2006-250

12. DISTRIBUTION/AVAILABILITY STATEMENT
Approved for public release; distribution is unlimited.

13. SUPPLEMENTARY NOTES
Conference paper postprint published in the Proceedings of the 41st AIAA/ASME/SAE/ASEE Joint Propulsion Conference and Exhibit.

PAO case number: AFRL/WS 05-1510; Date cleared: 27 Jun 2005.

14. ABSTRACT
An experimental investigation of a cascade injector was completed. The objective of this investigation was to determine whether the number of active stages in the cascade injector could be used to control penetration and mixing characteristics. The injector was tested at two overexpanded injection conditions in a Mach 3 crossflow. Shadowgraph and schlieren imaging, Mie scattering, Planar Laser Induced Fluorescence, and pressure profiling were the diagnostic techniques used to reveal various features of the injectant plume and its interaction with the supersonic crossflow. Results suggest that penetration can be controlled by the number of active stages in the cascade injector. Additional analysis and experiments are planned to better quantify the effects of injector stages revealed in this initial work.

15. SUBJECT TERMS
Supersonic combustion, fuel injection, laser-based diagnostics

16. SECURITY CLASSIFICATION OF:			17. LIMITATION OF ABSTRACT:	18. NUMBER OF PAGES	19a. NAME OF RESPONSIBLE PERSON (Monitor)
a. REPORT	b. ABSTRACT	c. THIS PAGE			Dr. Mark R. Gruber
Unclassified	Unclassified	Unclassified	SAR	22	19b. TELEPHONE NUMBER *(Include Area Code)* N/A

41st AIAA/ASME/SAE/ASEE Joint Propulsion Conference & Exhibit
10 - 13 July 2005, Tucson, Arizona

AIAA 2005-3708

Independent Stage Control of a Cascade Injector

H.L. Meicenheimer[*] and E.J. Gutmark[†]
Department of Aerospace Engineering
University of Cincinnati
Cincinnati, Ohio

C.D. Carter,[‡] D.R. Eklund,[§] and M.R. Gruber[‡]
Aerospace Propulsion Division, Air Force Research Laboratory
Wright Patterson AFB, Ohio

K.–Y. Hsu[**]
Innovative Scientific Solutions, Inc.
Dayton, Ohio

An experimental investigation of a cascade injector was completed. The objective of this investigation was to determine whether the number of active stages in the cascade injector could be used to control penetration and mixing characteristics. The injector was tested at two overexpanded injection conditions in a Mach 3 crossflow. Shadowgraph and schlieren imaging, Mie scattering, Planar Laser Induced Fluorescence, and pressure profiling were the diagnostic techniques used to reveal various features of the injectant plume and its interaction with the supersonic crossflow. Results suggest that penetration can be controlled by the number of active stages in the cascade injector. Additional analysis and experiments are planned to better quantify the effects of injector stages revealed in this initial work.

I. Introduction

One of the main factors governing combustion efficiency in a supersonic flowpath is the design of the fuel injection system. High flow velocities in the combustor result in very short residence times, thereby requiring mixing and combustion processes to occur rapidly. In a supersonic combustion ramjet (scramjet) the engine is operated at high equivalence ratios and with the minimum number of fuel injection sites practical. Each injector is designed to optimize between effective penetration into the high speed flow, and rapid mixing with the air. As a result, a variety of fuel injection techniques have been studied.

In the late 1960's, the structure of supersonic jets in relation to fuel injection to a scramjet began.[1-4] In the 1970's and 1980's research in this area expanded to include work investigating mixing and combustion of these flows.[5,6] Studies of structure, penetration, and mixing of supersonic jets have continued to the present.[7-11] Work involving staged injection concepts began in the late 1980's.[12-14] While much progress has been made, the behavior of this flowfield remains an active area of research today.

One current injection technique is the cascade injector developed by the Aerojet General Corporation.[15,16] This injector is a flush-mounted array of fourteen supersonic injectors, divided into four axial stages; each is supplied by a dedicated fuel manifold. The individual injector ports are aligned with the engine flow axis. Previous experimental studies indicated that this injector has excellent penetration characteristics.[15,16] However, in the relatively small test section used for this study, over-penetration and spanwise interactions between injection ports were observed. These features could limit the effectiveness of the cascade injector as initially designed.

---

[*] Graduate Student, Member AIAA.
[†] Ohio Eminent Scholar, Associate Fellow AIAA
[‡] Senior Aerospace Engineer, AFRL/PRAS, Associate Fellow AIAA.
[§] Aerospace Engineer, AFRL/PRAT, Senior Member AIAA.
[**] Senior Research Scientist, Senior Member AIAA.

Independent stage control has been suggested as one method to improve the effectiveness of the Aerojet cascade injector.[16] By examining combinations of active stages while maintaining a constant injection pressure condition (i.e., constant mass flow rate through each stage), the effects on penetration and mixing may be observed. This topic is the subject of the current work. Shadowgraph and schlieren imaging, Mie scattering, Nitrogen Oxide-Planar Laser Induced Fluorescence (NO-PLIF), and pressure profiling were the diagnostic techniques used to reveal various features of the injectant plume and its interaction with the supersonic crossflow.

II. Experimental Facility and Instrumentation

The AFRL/PRAS Research Cell 19 facility (RC19) is a modular test facility used for studies of fuel injection, inlet-combustor interactions, and flameholding in supersonic flows. A full description of the facility and its capabilities are found in Reference 17. A picture and schematic of RC19 appear as Figs. 1a and 1b, respectively. For the present experiments, the nozzle block assembly provides a nominal facility Mach number of M = 3. The test section is 2.0 inches high by 6.0 inches wide. The bottom wall, where the injector is mounted, has a 2.5 degree divergence. Fused silica windows mounted in the other three walls provide optical access to the test section. The laboratory contains a state-of-the-art pressure scanning system, and probe-based instrumentation. The facility is also equipped to perform instantaneous and time-averaged flow visualization techniques as well as laser-based diagnostic techniques.

Fuel Injection Hardware

The cascade injector block used in this study was originally designed to be strut-mounted with injection ports on both sides. The injection block was modified for testing in RC19, and is shown in Fig. 2.[15,16] Although three injectors are shown in Fig. 2, only the center injector is used in the current study. The center injector is a single cascade composed of fourteen injection ports that are grouped into four axial stages. Each stage is independently supplied with fuel; the fuel supplied to each stage can be turned on and off with a ball valve.

Stagnation temperature is measured in the fuel manifold prior to the injection block. Stagnation pressure is also measured for each stage to allow preservation of a constant injection pressure and mass flow rate condition. The nominal injection pressures used for these experiments were 144 psia and 250 psia, which correspond to overexpanded injection conditions. The lower pressure condition was selected so that the baseline condition, where all four stages are active, could be compared with previous experimental results.[16] The higher pressure condition was selected based on the upper limit of RC19 at the time of the experiments (NO supply pressure limitation).

NO-PLIF Diagnostic

To excite NO molecules, a laser system generated radiation at 226 nm, to tune to the $R_1(8.5)$ transition of the $A^2\Sigma^+$ ($v' = 0$) $\leftarrow$ $X^2\Pi_i$ ($v'' = 0$) band. A frequency-doubled, injection-seeded Nd:YAG pumped a Lumonics Hyperdye (HD-300) dye laser. The output of the Hyperdye (574 nm) was frequency doubled, using an Inrad Autotraker, and the doubled radiation was then frequency mixed with the residual infra-red beam from the Nd:YAG, within a second Autotraker, to produce laser radiation at 226 nm. The 3-mJ/pulse 226-nm beam was then directed to an optical table located beneath the wind tunnel test section; this table is placed on a three-dimensional traversing system. The laser beam path was parallel to the tunnel's axial coordinate, so that the laser sheet could be accurately placed at the desired axial position.

To form a sheet, a two-lens telescope was used: a negative cylindrical lens (-50 mm focal length) followed by a positive spherical lens (1 m focal length), as shown in Fig. 3. The minimum sheet thickness occurred within the tunnel, and the sheet height, at about 75 mm, was nearly constant. The sheet normal was rotated 2.5 degrees to be parallel to the tunnel bottom wall. Fluorescence was imaged using a Princeton Instruments "Superblue" PIMAX intensified CCD (charge-coupled device) camera, which was fitted with a fast Cerco 45-mm, f/1.8 lens. A Schott glass UG-5 filter was used to block scattering at 226 nm—and fluorescence from the (0,0) band—and pass fluorescence from the A-X (0,1), (0,2), (0,3), … bands. For the "end-view" imaging of the plume, the laser probe region was not normal to the camera axis. Thus, to mitigate image blur, a schiempflug mount was used. Camera pixels were binned 2 by 2, to improve signal strength, resulting in an effective array size of 256 by 256 pixels.

The NO concentration within the bottle was at 1% (or 10,000 parts per million, PPM) in N_2. Before injection into the tunnel, the NO-laden N_2 was diluted with air such that the NO/N_2 mole fraction within the injectant was about 2%. Thus, the NO concentration in the jet as it entered the tunnel was about 200 PPM, an amount

sufficient for strong fluorescence signals. To ensure proper operation of the laser system during the test, the beam energy and wavelength were continuously monitored. A small portion of the 226-nm beam was split off and directed over a small CH_4-air burner (to generate NO)—with fluorescence measured with a photomultiplier tube—and then to a fast photodiode. An oscilloscope displayed both signals, and the laser was adjusted to keep the signals constant throughout the test.

Data Collection and Analyses

The test matrix, shown in Table 1, consisted of 11 stage combinations and two nominal injection pressure conditions. NO-PLIF was used to examine penetration in the cross-flow plane. At each injection condition, the laser sheet was transmitted perpendicular to the injection plate at seven axial locations: x = -0.5, 0.0, 0.5, 1.0, 1.5, 2.0, and 2.5 inches relative to the middle of the 14th injection port of the cascade. An ensemble of 200 end-view NO-PLIF images was collected at each location and injection condition. Background images with no injection were also taken at each location. The field of view for these images was 1.75 inches high by 3.5 inches wide. For viewing the profile of the injector plume, the laser sheet was transmitted thru the top window at the spanwise centerline of the injector. The field of view for these images was 2.5 inches high by 3.0 inches long. Again, 200-image ensembles were obtained along with background images.

For the results reported in this paper, the raw end view images were processed in several steps. First, each image in the ensemble was corrected for perspective distortion using an image of a dot card with known spacing between the dots. Plume images were normalized by recording NO PLIF images with the tunnel uniformly seeded with NO (with no flow in the tunnel). Each image was then divided by this reference image, removing the effects of laser sheet intensity distribution, collection efficiency, and camera fixed pattern noise. The background image was subtracted from each plume image, then the images were averaged and the standard deviation was determined. Each average image was normalized by the maximum NO signal. Penetration distance and the maximum injection plume width were identified for each case. For this study, the penetration distance was defined to be the maximum vertical position having at least 10% of the maximum signal. Maximum injection width was the largest difference between the first and last occurrence of 10% of the maximum signal at a given transverse position in the jet plume.

A per unit mass comparison was completed to determine the effects of each stage on penetration distance. An influence coefficient (IC) representing the sensitivity of penetration distance to mass flow for each case was defined in the following manner:

$$IC = \frac{\Delta y / y}{\Delta \dot{m} / \dot{m}} \tag{1}$$

where y is the penetration distance of the baseline case, Δy is the difference in penetration distances between the baseline case and the particular case of interest, $\dot{m}$ is the mass flow rate of the baseline case, and $\Delta\dot{m}$ is the difference in mass flow between the baseline case and the case of interest. Note that mass flow is defined:

$$\dot{m}_i = \rho u \sum\nolimits_i (A^* Cd)_i \tag{2}$$

where i represents the stage number. Note that the quantity (ρu) is the same for each case and cancels out in the division of $\Delta\dot{m}$ and $\dot{m}$.

III. Results and Discussion

Injectant Plume Structure

In Figure 4a, the axial development of the instantaneous injection plume for Case 1 is shown for a nominal injection pressure of 144 psia. In these images, dark regions correspond to freestream fluid (i.e., fluid with no nitric oxide). Bright regions, on the other hand, are indicative of fluid with nitric oxide at some detectable concentration. The plume emerges as a thin initial jet that spreads and lifts away from the wall as it moves downstream from the injector. The penetration of the plume increases slowly until reaching a relatively constant penetration distance near the x = 1.0 inch position. The width of the injection plume remains relatively constant as the downstream axial position increases. As shown in the raw (unprocessed) side-view NO PLIF image in Figure 4b, a structure of vortices following the bow shock develops into a turbulent shear layer at a constant height. Standard deviation images are shown in Figure 4c. In these images, light regions correspond to high levels of standard deviation. These regions can be considered to be where large-scale mixing between the jet and crossflow fluids is taking place.

Dark regions indicate low levels of standard deviation. These images indicate relatively high levels of unsteadiness at the interface between the injectant and air in the crossflow. Ensemble-averaged images are shown in Figure 4d. In these images, the plume begins as a 2-dimensional conical structure that spreads into an oval as it lifts away from the wall and moves downstream; behavior that is consistent with that shown in Figure 4a.

Similar plume behavior is seen in Figures 5a and 5b, which show the effects of increased injection pressure on Case 1. In Figure 5a, the instantaneous injection plume is shown. Figure 5b shows ensemble-averaged images. The plume structure and development in both figures is similar to those in Figures 4a and 4d. However, in this case, the plume shape begins as a cylinder and develops into a 2-dimensional conical structure as axial position increases and the plume appears to lift farther from the wall. Penetration distance is observed to increase significantly as a result of the increased injection pressure, but the maximum injection plume width is not as significantly affected by this increase.

Plume Penetration and Spreading

Case 1, with 4 active injection stages, was used as a baseline for comparing the effects of active injection stages on the penetration and spreading of the plume. Raw and ensemble-averaged images for Case 1 were discussed above for two injection pressure conditions (Figs. 4a and 4d for 144 psia and Figs. 5a and 5b for 250 psia). In both cases, the penetration distance increased to a relatively constant value near the x = 1.0 inch position and maximum plume width was observed to continually increase with increasing downstream position. Note that penetration and plume spread increased in response to higher injection pressure. Figures 6 and 7, respectively, show the penetration profiles and maximum plume width resulting from the analysis of the processed images shown in Figs. 4d and 5b. These profiles will be referred to as baseline cases in subsequent figures. In Figure 6, an initially rapid growth rate slowed as downstream position increased for both injection conditions. Penetration distance was observed to be approximately 1.0 inch for the lower injection pressure case, and 1.5 inches for the case with higher injection pressure. This behavior is consistent with previous experimental results.[16] Figure 7 shows plume width to continually increase with increasing downstream position, ending at 0.73 inches for the lower injection pressure case and 0.79 inches for the case with higher injection pressure.

Figure 8 presents a comparison of the cases with three active stages with an injection pressure of 144 psia. The maximum penetration distance of y = 0.94 inches occurred for Case 4. The minimum penetration of y = 0.83 inches occurred in Case 2. Case 3 had a final penetration distance of y = 0.90 inches, which was slightly greater than the final penetration distance of y = 0.85 inches for Case 5. The penetration distance in Figure 8 appears to be most significantly affected by stages 1 and 4. The first stage of the cascade is important because it "shields" the downstream stages by absorbing the initial force of the crossflow. This shield sets up a shock structure, which enables downstream stages to penetrate farther into the crossflow. The importance of stage 4 is demonstrated by the observed increase in penetration distance between Case 2 and Case 5.

The penetration distance hierarchy observed in Fig. 8 is more easily seen in Fig. 9 where the cases with three active injection stages at the higher nominal injection pressure are plotted. The cases, ranked in order of maximum to minimum penetration distance are: Case 4, Case 3, Case 5, and Case 2. This ranking appears to indicate that stage 1 has a slightly higher impact on penetration than stage 4; Case 2 penetrates slightly farther than Case 5 at the higher injection pressure condition. The significantly higher penetration distance of Case 4 compared with Case 5 in this figure effectively shows the importance of stage 1.

In Fig. 10, the cases having two active stages and an injection pressure of 144 psia are compared. The cases, ranked in order from maximum to minimum penetration distance were: Case 8, Case 10, Case 11, Case 9, Case 6, and Case 7. The maximum final penetration distance for these cases was y = 0.75 inches, observed in Case 8. The minimum final penetration distance of y = 0.66 inches occurred in Case 9. Again, the penetration distances illustrate the importance of stages 1 and 4.

Although Figs. 8 through 10 indicate that stage 4 has a notable impact on penetration distance, Tables 2 and 3 indicate that this stage does not have a significant effect on the penetration distance on a per mass basis. For the cases with three active stages at an injection pressure of 144 psia (Table 2), the stages that had an effect on penetration distance per unit mass in order from maximum to minimum effect were: stage 1, stage 2, stage 3, and stage 4. The stages that had an effect on penetration distance per unit mass at an injection pressure of 250 psia in order from greatest to least effect were: stage 1, stage 2, stage 4, and stage 3. Note that the influence coefficients of

stages 3 and 4 in Table 2 are very close in value. This similarity is expected because stages 3 and 4 have comparable mass flow rates. The cases having 2 active stages and an injection pressure of 144 psia, ranked from maximum to minimum effect on penetration distance per mass as indicated by the influence coefficients in Table 3 are: Case 11, Case 10, Case 8, Case 7, Case 9, and Case 6. This ranking indicates that the combination of stages having the most effect on penetration distance per unit mass was stages 1 and 2. The combination of stages having the least effect on penetration distance per unit mass was stages 3 and 4. This ranking is consistent with the effects shown in Table 2. The influence coefficients shown in Tables 2 and 3 suggest that the aerodynamic characteristics of stages 1 and 2 are very important when considering the penetration of this injector design. That is, despite having the smallest mass flow rates, stages 1 and 2 appear to have the most pronounced impact on penetration distance.

The maximum injectant plume width as a function of axial location for all cases, are shown in Figs. 11 through 13. Figure 11 is the plume width data for cases having three active stages at an injection pressure of 144 psia. Figure 12 presents the plume width data for the cases having three active stages and an injection pressure of 250 psia. In Fig. 13 the plume width data for cases having 2 active stages at an injection pressure of 144 psia is shown. In all cases, the maximum injectant plume width increases as axial location progresses downstream; a trend which is attributed to mixing.

The height of the maximum injectant plume width was also plotted as a function of axial location for all cases. Figure 14 presents the data for cases having three active stages at an injection pressure of 144 psia. Figure 15 displays data for cases having three active stages at an injection pressure of 250 psia. In Fig. 16, the data for cases having 2 active stages at an injection pressure of 144 psia is shown. At this time, no explanation is offered for the oscillations observed in these cases. Ongoing CFD simulations and analysis of additional data may yield an explanation for this behavior.

IV. Conclusions and Recommendations

Based on end-view NO PLIF images, the penetration distance of the cascade injector was measured for a variety of staging schemes. Preliminary results indicate that the first and fourth stages are critical; when these stages are not active, the penetration distance decreases. Analyses of the side-view NO PLIF, shadowgraph and schlieren images, Mie scattering images, and pressure profiling data gathered during this investigation, as well as an improved analysis of the spanwise data are underway. Additionally, an experimental study employing Raman Scattering on a reduced test matrix to obtain quantitative mixing information is planned. CFD simulations of various conditions are also in progress. These simulations should provide additional insights into the mechanics governing the penetration and mixing characteristics of the cascade injector.

V. Acknowledgements

This work was sponsored by Dr. J. Tishkoff with funding provided by the Air Force Office of Scientific Research. The cascade injector was provided by Mr. M. Bulman of Aerojet General Corporation. The authors gratefully acknowledge D. Schommer and W. Terry for their contributions to experimental set-up, testing, and overall laboratory support during this project. They also thank G. Streby for his design and engineering support. Support from the Research Air Facility and the ASC MSRC Department of Defense High Performance Computing Center at Wright Patterson AFB is also recognized and appreciated.

VI. References

1. Zukoski, E.E., and Spaid, F.W., "Secondary Injection of Gases into a Supersonic Flow." *AIAA Journal*, Vol. 2, No. 10, 1964, pp. 1689-1696.
2. Schetz, J.A., and Billig, F.S., "Penetration of Gaseous Jets Injected into a Supersonic Stream." *Journal of Spacecraft*, Vol. 3, No. 11., 1966, pp. 1658-1665.
3. Schetz, J.A., Hawkins, P.F., and Lehman, H., "Structure of Highly Underexpanded Transverse Jets in a Supersonic Stream." *AIAA Journal*, Vol. 5, No. 3, 1967, pp. 882-884.
4. Schetz, J.A., Weinraub, R.A., and Mahaffety Jr., R.E., "Supersonic Transverse Injection into a Supersonic Stream." *AIAA Journal*, Vol. 6, No. 3, 1968, pp. 933-934.
5. Brown, G.L., and Roshko, A., "On Density Effects and Large Structure in Turbulent Mixing Layers." Journal of Fluid Mechanics, Vol. 64, Part 4, 1974, pp. 775-816.
6. Schetz, J.A., Billig, F.S., and Favin, S., "Analysis of Mixing and Combustion in a Scramjet Combustor with a Co-Axial Fuel Jet." AIAA Paper 80-1256, 1980.

7. Fric, T.F, and Roshko, A., "Vortical Structure in the wake of a Transverse Jet." Journal of Fluid Mechanics, Vol. 279, 1994, pp. 1-47.
8. Gruber, M.R., Chen, T.H., and Nejad, A.S., "Mixing and Penetration Studies of Sonic Jets in a Mach 2 Freestream." Journal of Propulsion and Power, Vol. 11, No. 2, 1995, pp. 315-323.
9. Everett, D.E, and Dutton, J.C., "Pressure-Sensitive Paint Measurements of the Pressure Field about a Sonic Jet Injected Transversely into a Mach 1.6 Freestream." AIAA Paper 95-0524. 1995.
10. Gruber, M.R., Nejad, A.S., Chen, T.H., and Dutton, J.C., "Bow Shock/Jet Interaction in Compressible Transverse Injection Flowfields." *AIAA Journal*, Vol. 34, No. 10, 1996, pp. 2191-2193.
11. Gruber, M.R., Nejad, A.S., Chen, T.H., and Dutton, J.C., "Compressibility Effects in Supersonic Transverse Injection Flowfields." *Physics of Fluids*, Vol. 9, No. 5, 1997, pp. 1448-1461.
12. Hollo, S.D, Hartfield Jr., R.J., and McDaniel, J.C., "Injectant Mole Fraction Measurements of Transverse Injection in Constant Area Supersonic Ducts." AIAA Paper 90-1632, 1990.
13. Hollo, S.D, McDaniel, J.C., and Hartfield Jr., R.J., "Quantitative Investigation of Compressible Mixing: Staged Transverse Injection into Mach 2 Flow." *AIAA Journal*, Vol. 32, No. 3, 1994, pp. 528-534.
14. Eklund, D.R., Northam, G.B., Dancey, C.L., and Wang, J.A., "Computational/Experimental Investigation of Staged Injection into a Mach 2 Flow." *AIAA Journal*, Vol. 32, No. 5, 1994, pp. 907-916.
15. Cox-Stouffer, S.K., Gruber, M.R., and Bulman, M.J., "A Streamlined, Pressure-Matched Fuel Injector for Scramjet Applications," AIAA Paper 2000-3707, 2000.
16. Mathur, T., Cox-Stouffer, S., Hsu, K.-Y., Crafton, J., Donbar, J., and Gruber, M., "Experimental Assessment of a Fuel Injector for Scramjet Applications," AIAA Paper 2000-3703, 2000.
17. Gruber, M.R., and Nejad, A.S., "New Supersonic Combustion Research Facility," *Journal of Propulsion and Power*, Vol. 11, No. 5, 1995, pp. 1080-1083.

Table 1: Experimental test matrix.

Case #	Active Stages	Nominal Injection Pressure (psia)
1	1,2,3,4	144, 250
2	1,2,3	144, 250
3	1,2,4	144, 250
4	1,3,4	144, 250
5	2,3,4	144, 250
6	1,2	144
7	1,3	144
8	1,4	144
9	2,3	144
10	2,4	144
11	3,4	144

Table 2: IC's for cases with 3 active stages

Case #	Influence Coefficient P_{inj} = 144 psia	Influence Coefficient P_{inj} = 250 psia
2	0.466	0.570
3	0.511	0.558
4	0.787	0.963
5	1.53	1.97

Table 3: IC's with 2 active stages

Case #	Influence Coefficient P_{inj} = 144 psia
6	0.499
7	0.619
8	0.688
9	0.611
10	0.766
11	1.19

Figure 1a: Picture of RC19 facility

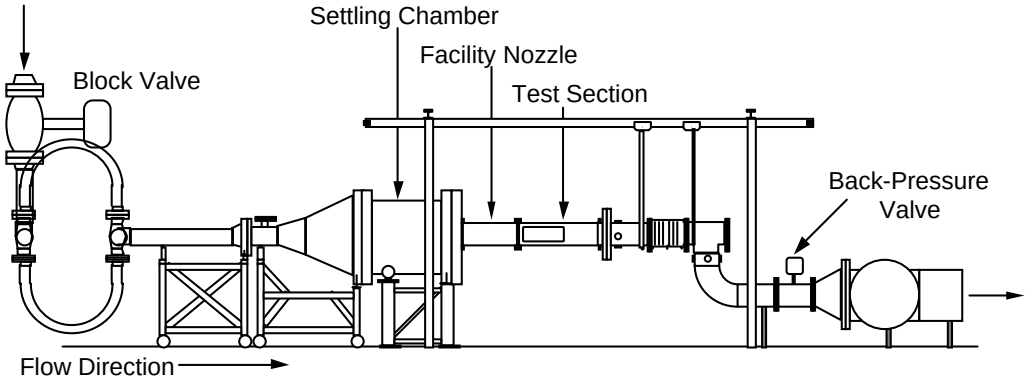

Figure 1b: RC19 facility schematic

Figure 2: Aerojet cascade injector block

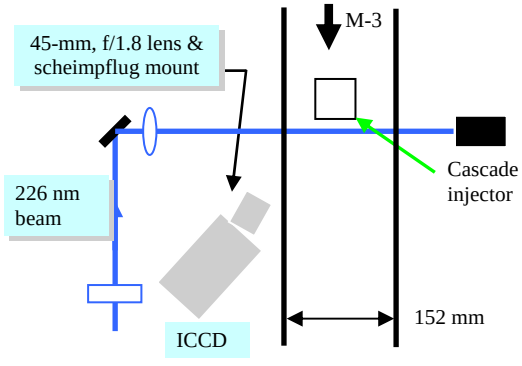

Figure 3: RC19 optics layout.

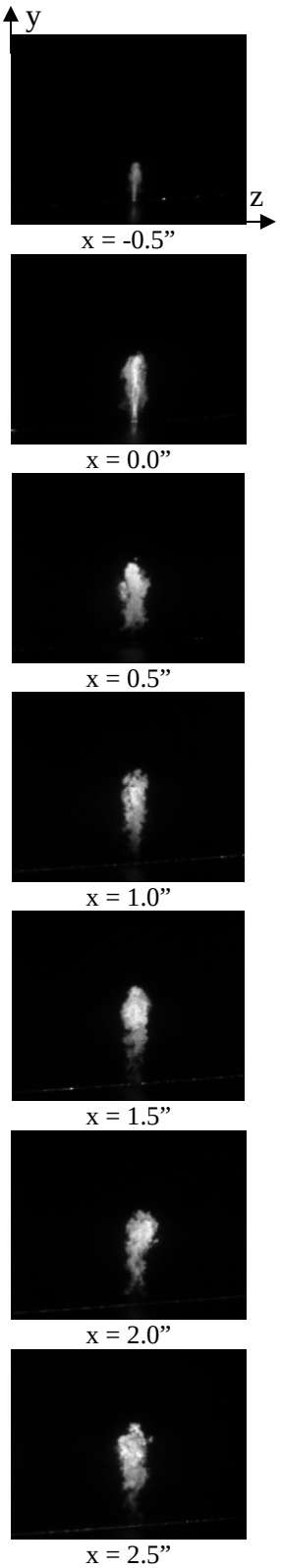

Figure 4a: Axial development of injectant plume in instantaneous images (Case 1, P_{inj} = 144 psia)

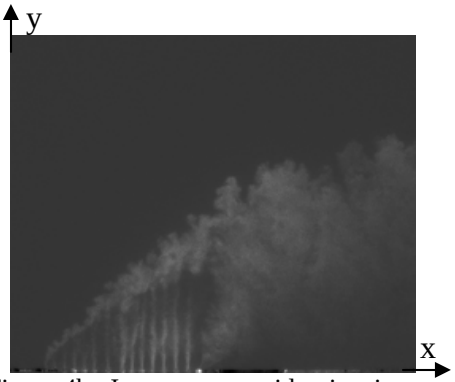

Figure 4b: Instantaneous side-view image (Case 1, P_{inj} = 144 psia)

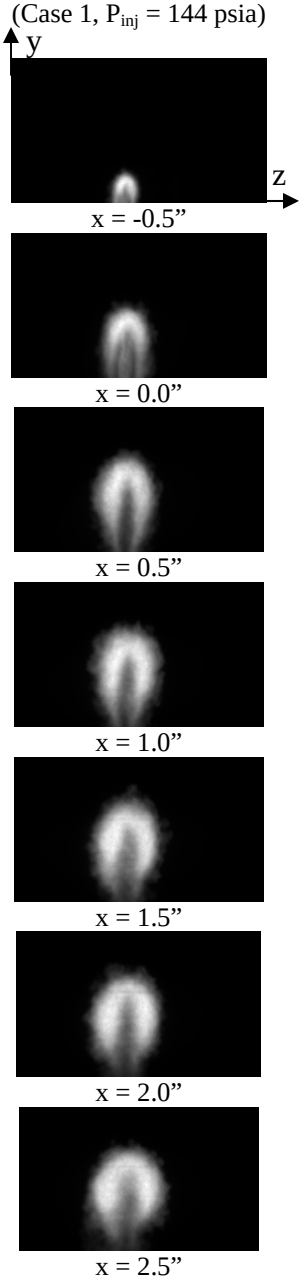

Figure 4c: Axial development of standard deviation (Case 1, P_{inj} = 144 psia)

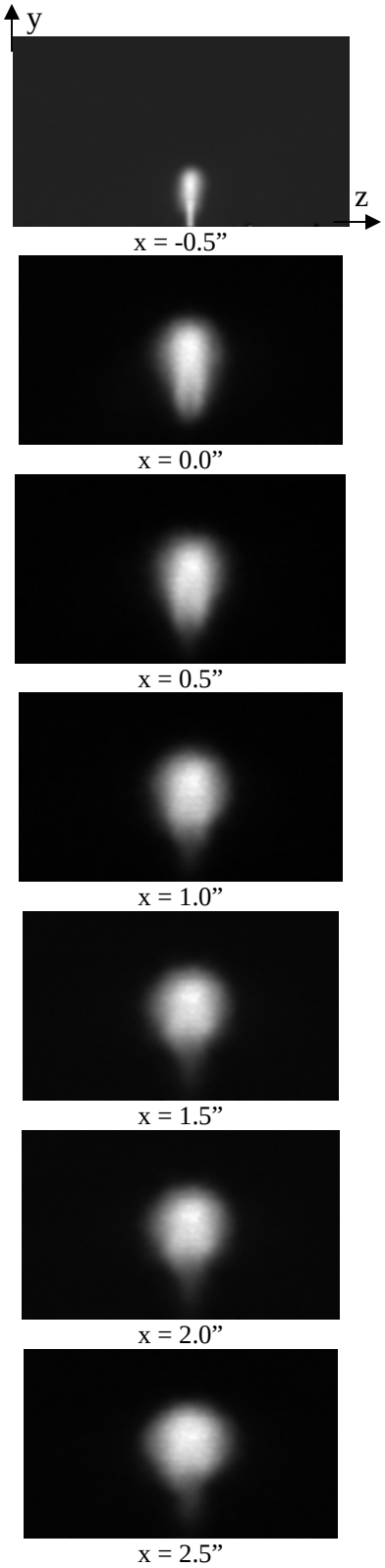

Figure 4d: Axial development of injectant plume in processed images (Case 1, P_{inj} = 144 psia)

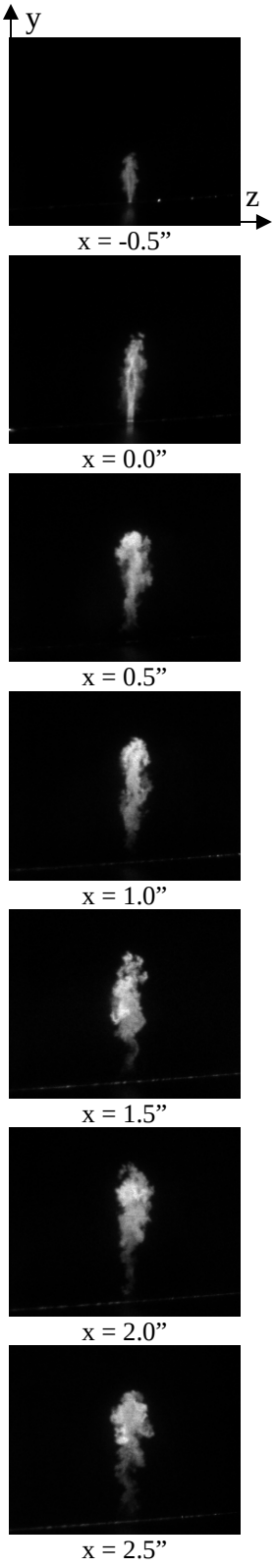

Figure 5a: Axial development of injectant plume in instantaneous images (Case 1, P_{inj} = 250 psia)

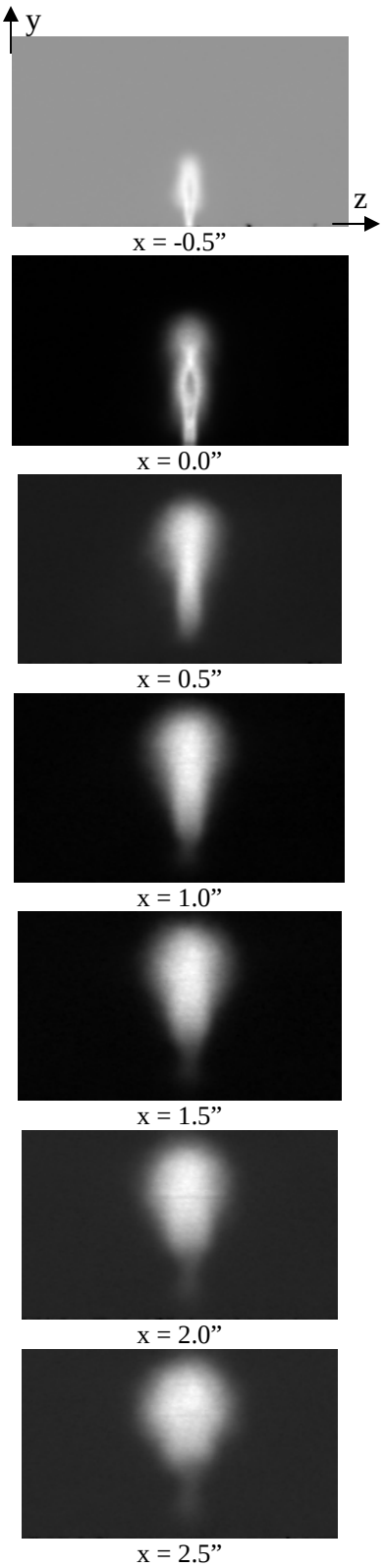

Figure 5b: Axial development of injectant plum in processed images (Case 1, P_{inj} = 250 psia)

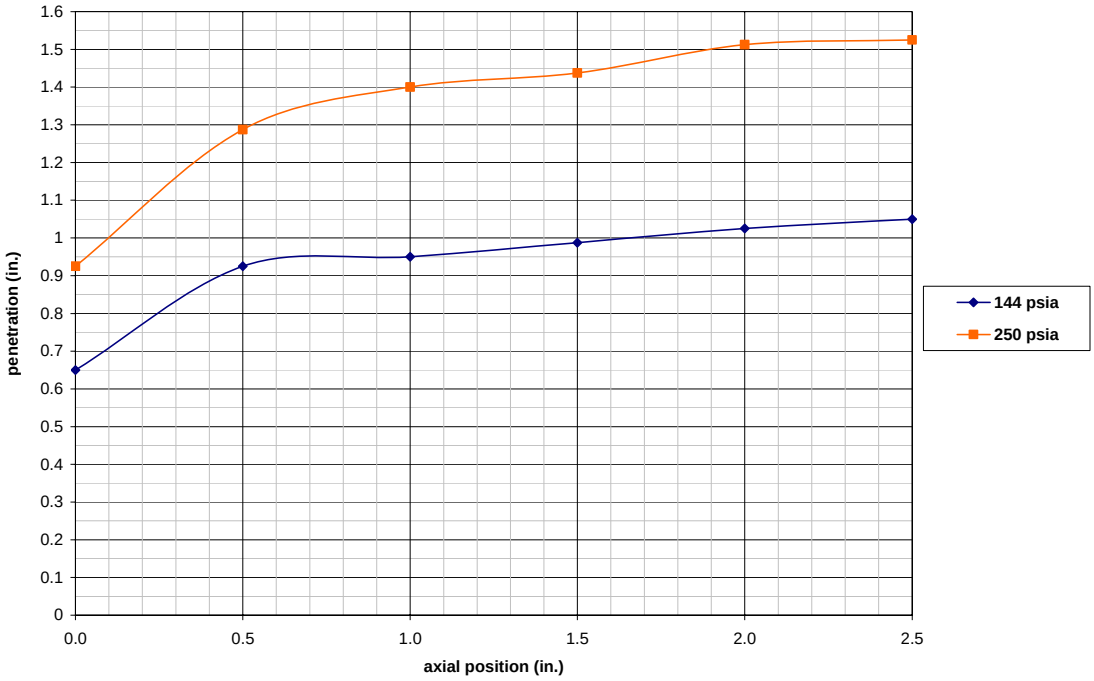

Figure 6: Transverse penetration profiles for baseline cases.

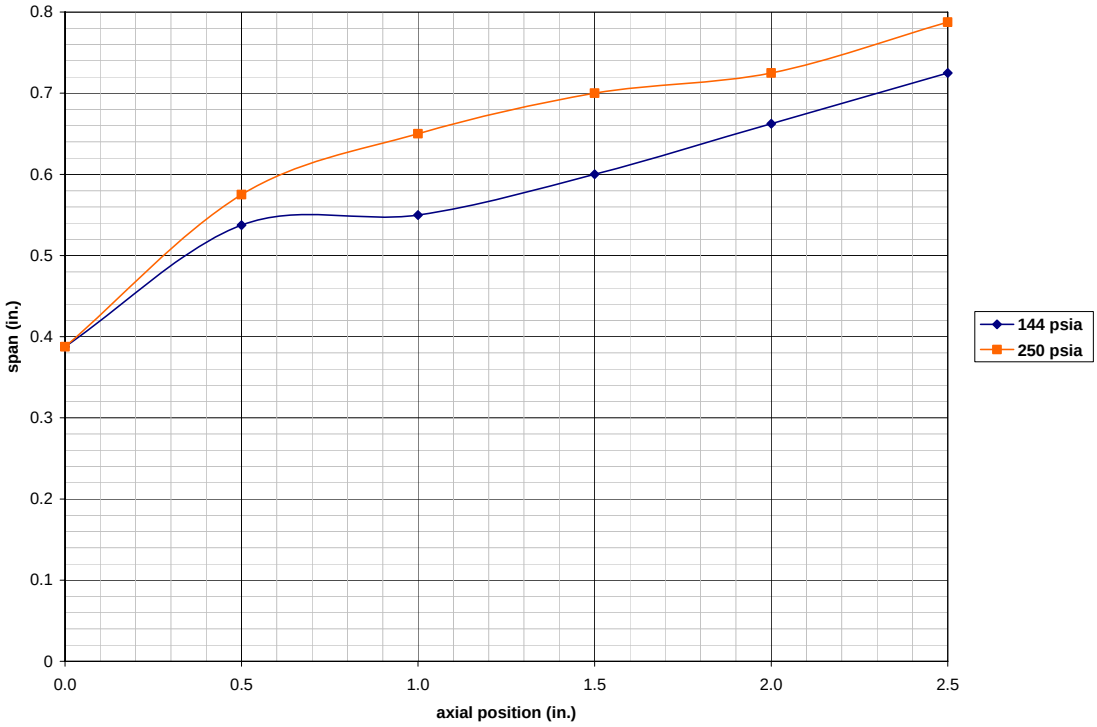

Figure 7: Maximum plume width profiles for baseline cases.

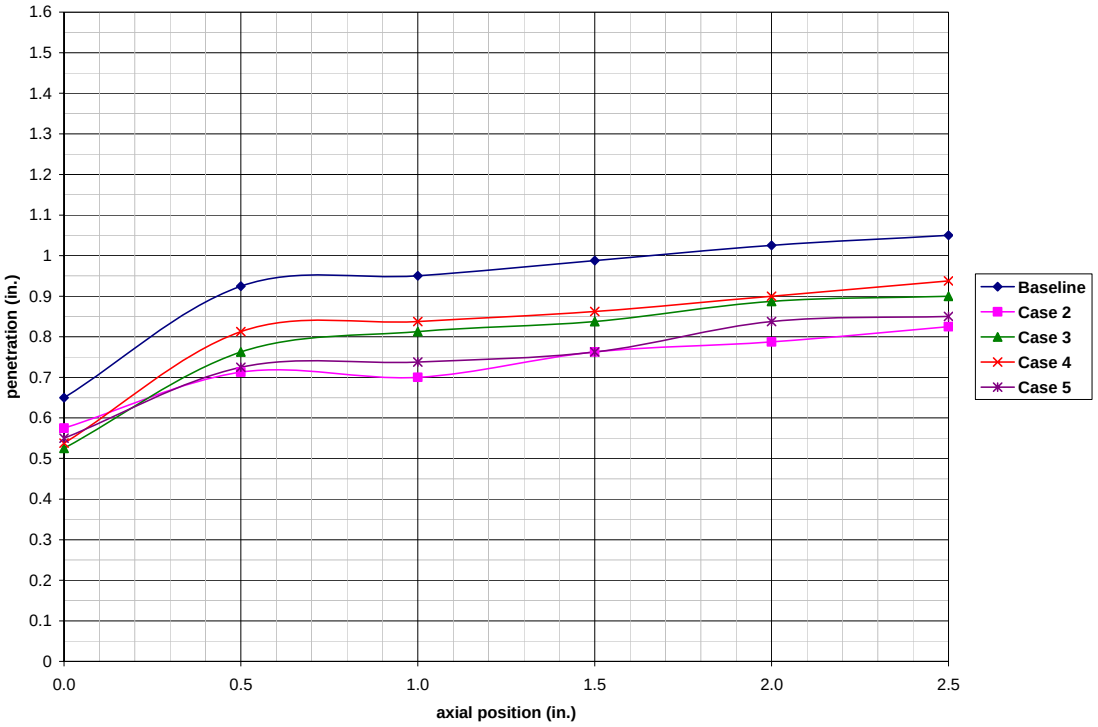

Figure 8: Transverse penetration profiles for cases with 3 active stages, P_{inj} = 144 psia

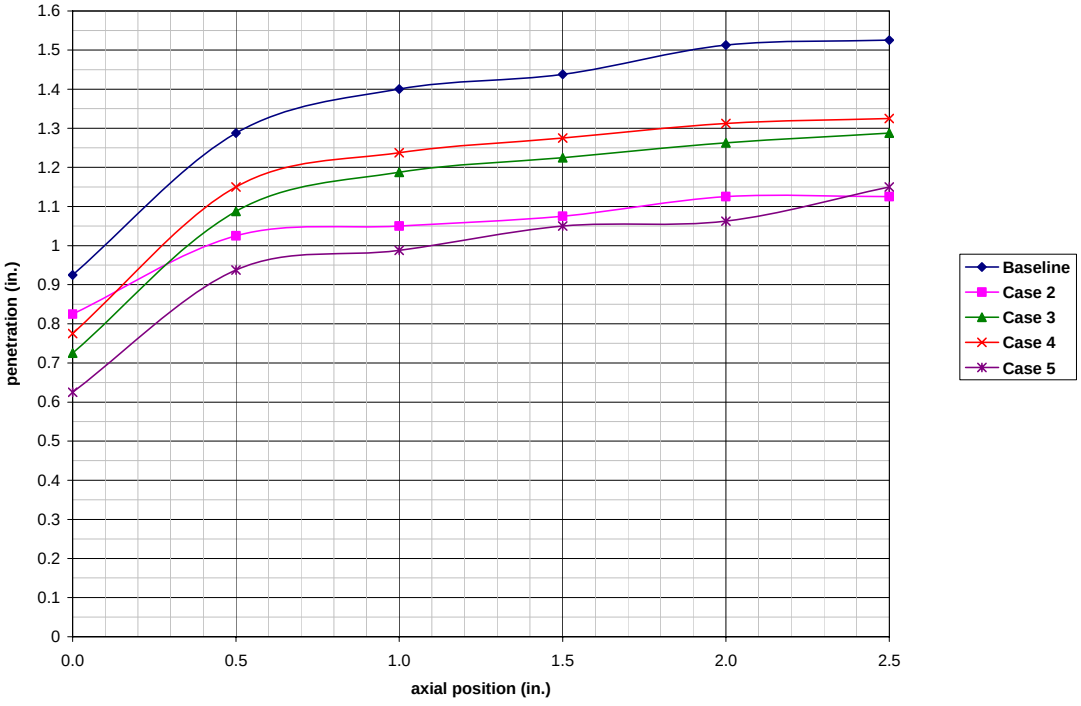

Figure 9: Transverse penetration profiles for cases with 3 active stages, P_{inj} = 250 psia

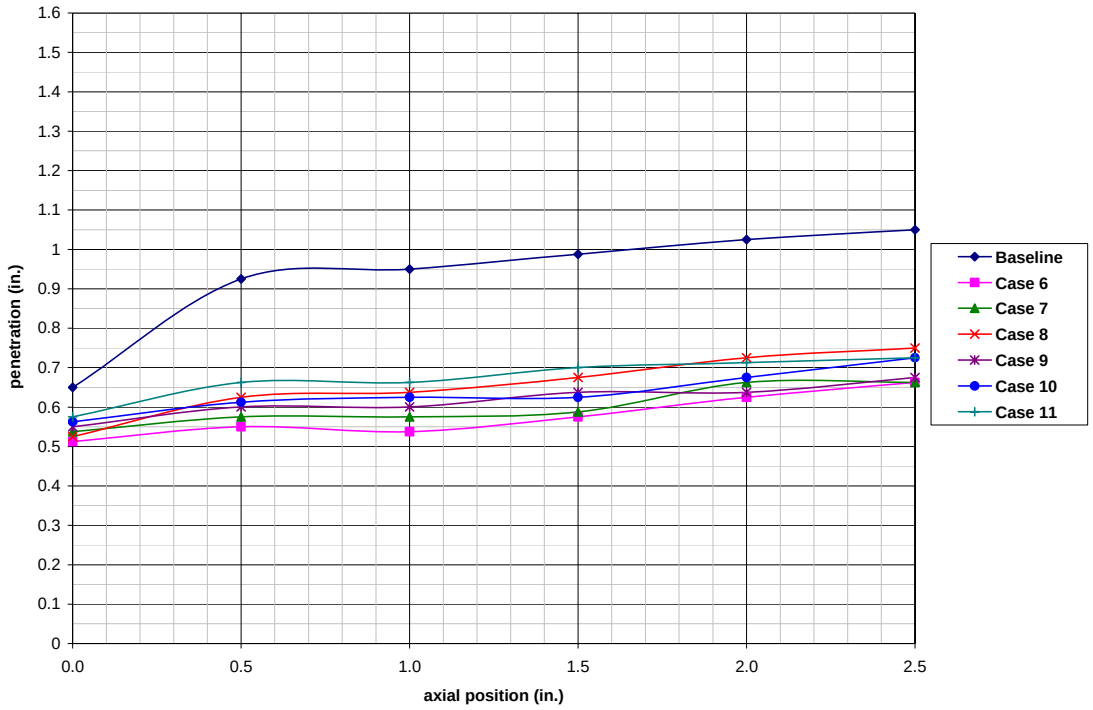

Figure 10: Transverse penetration profiles for cases with 2 active stages, P_{inj} = 144 psia

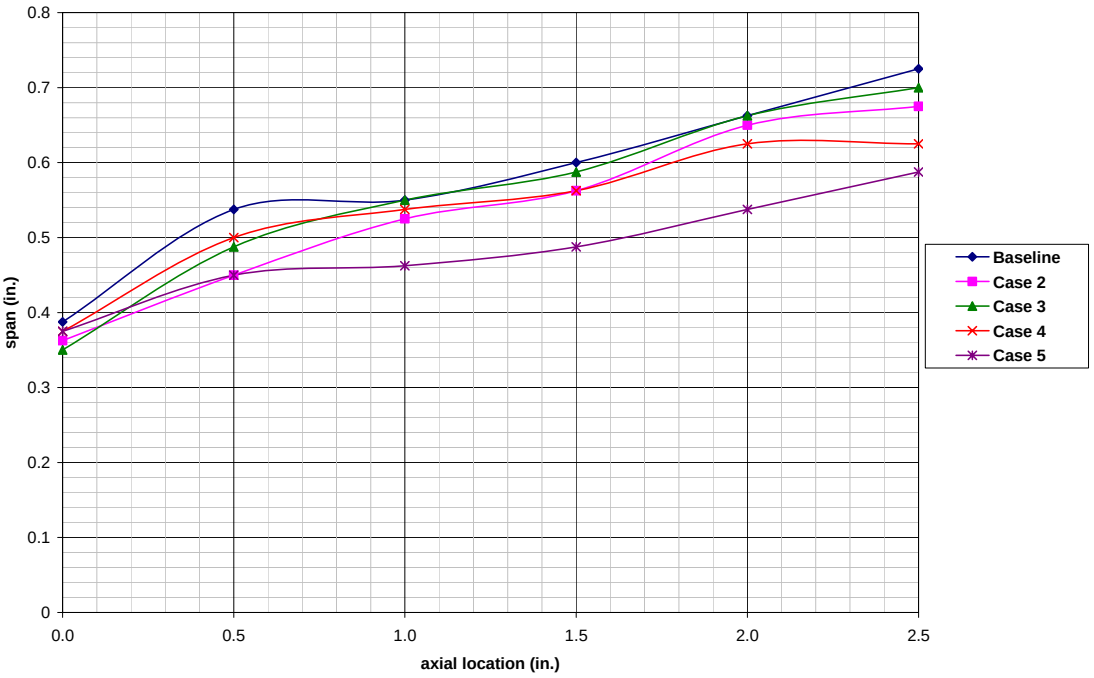

Figure 11: Maximum injectant plume width for cases with 3 active stages, P_{inj} = 144 psia

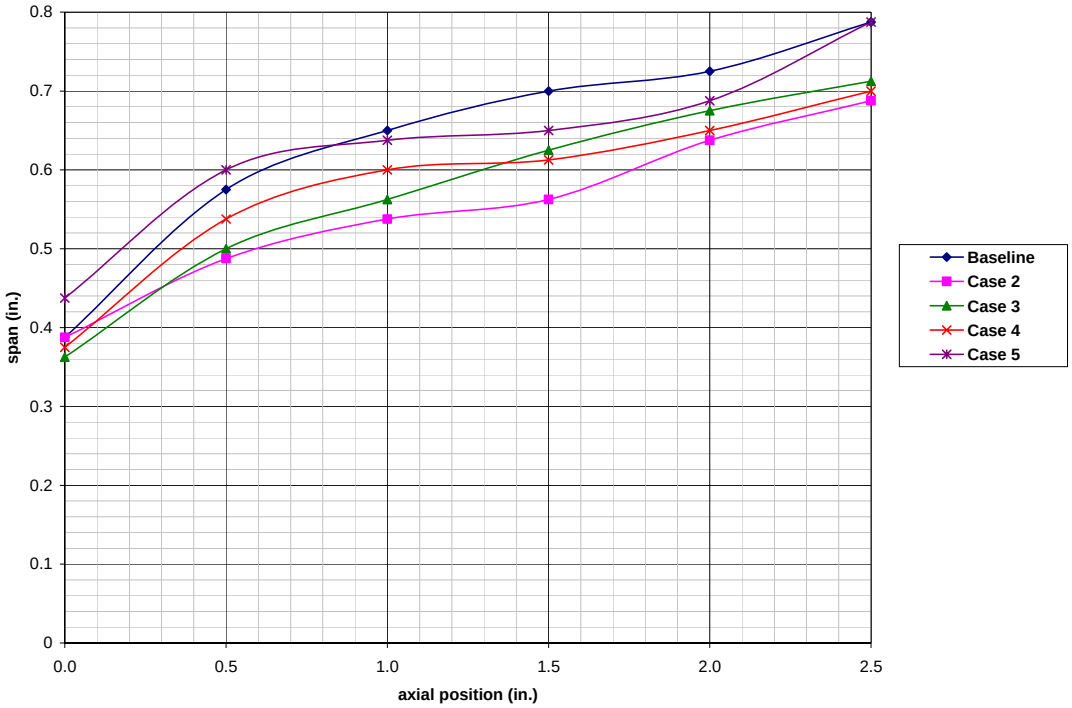

Figure 12: Maximum injectant plume width for cases with 3 active stages, P_{inj} = 250 psia

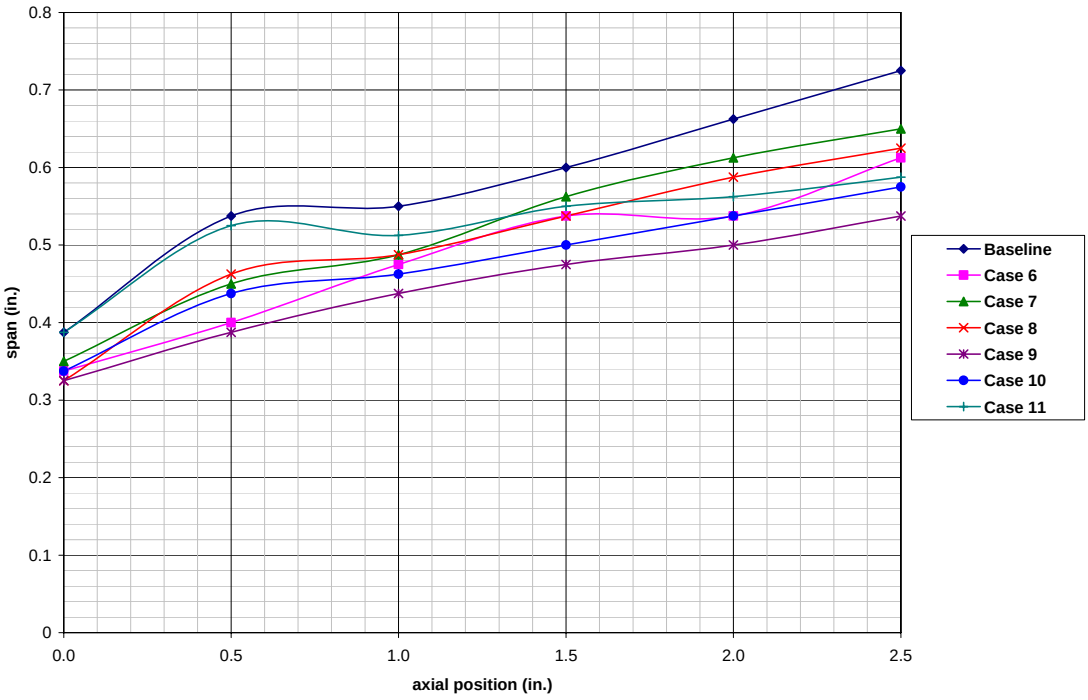

Figure 13: Maximum injectant plume width for cases with 2 active stages, P_{inj} = 144 psia

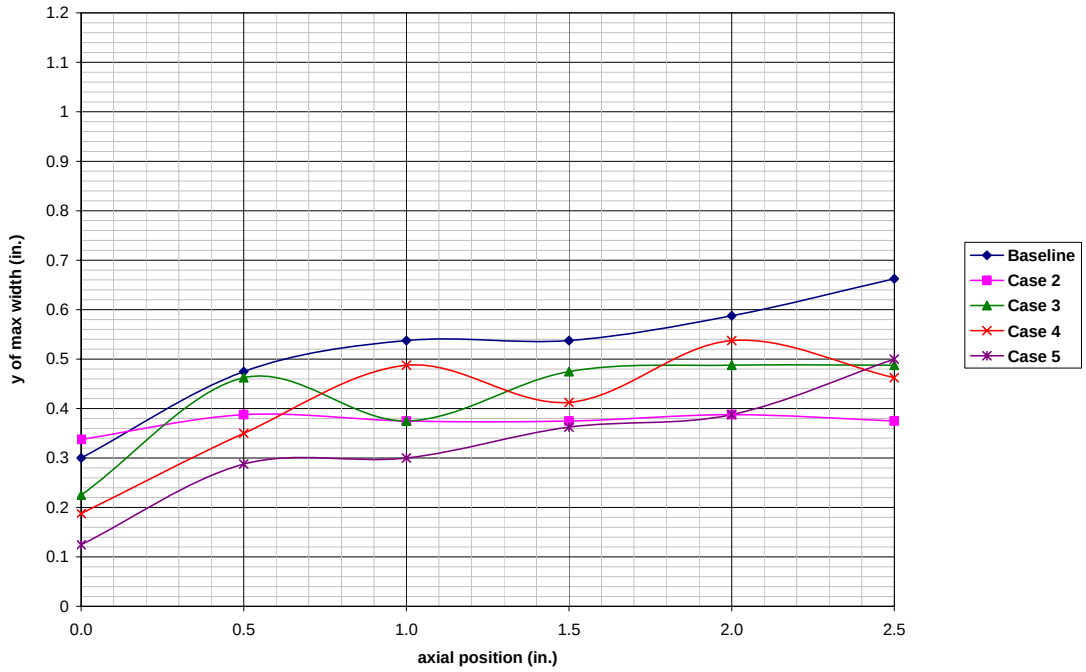

Figure 14: Height of maximum injectant plume width for cases with 3 active stages, P_{inj} = 144 psia

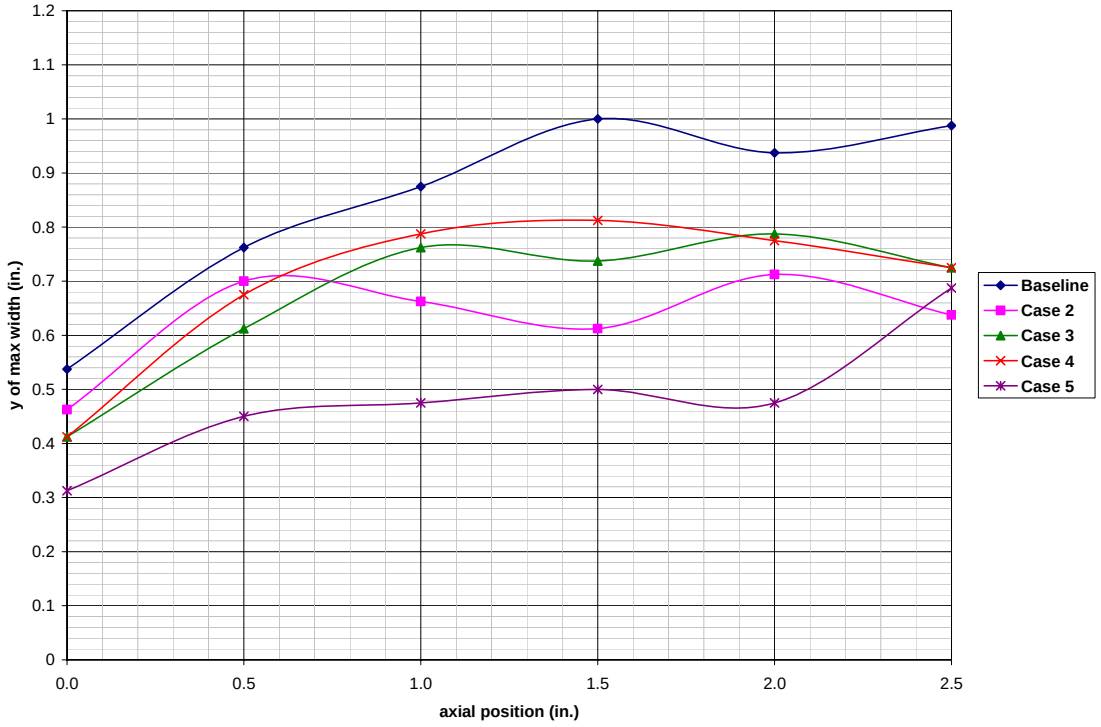

Figure 15: Height of maximum injectant plume width for cases with 3 active stages, P_{inj} = 250 psia

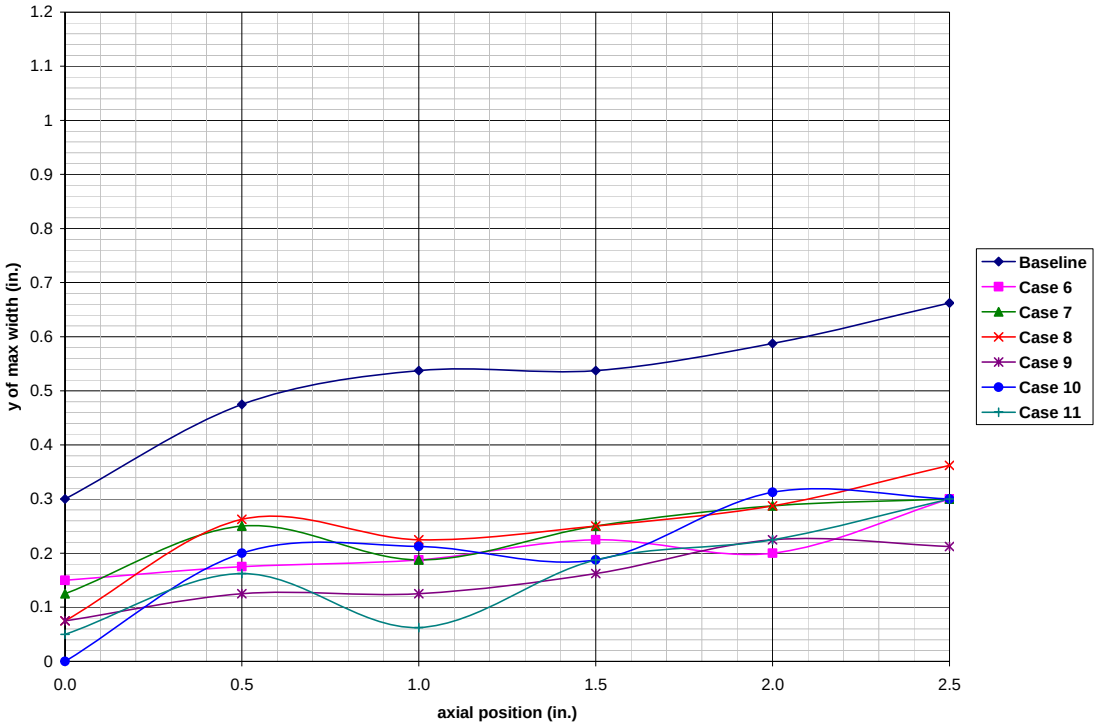

Figure 16: Height of maximum injectant plume width for cases with 2 active stages, P_{inj} = 144 psia